Relaxation Kinetics During Aging of a Float Glass

By

SHANNON JURCA

THESIS

Submitted in partial satisfaction of the requirements for the degree of

MASTER OF SCIENCE

in

Materials Science and Engineering

in the

OFFICE OF GRADUATE STUDIES

of the

UNIVERSITY OF CALIFORNIA

DAVIS

Approved:

Sabyasachi Sen, Chair

Subhash Risbud

Ricardo Castro

Committee in Charge

2021

Abstract

The relaxation behavior of different properties such as stress, volume and structure are known to be strongly coupled in silicate glasses and liquids. However, recent studies have raised the question as to whether the relaxation behavior of these properties are truly equivalent. In this study, density, Raman spectroscopy and viscosity measurements are utilized to probe, respectively, the volume, structural and shear relaxation behaviour of a soda lime silicate glass of standard float composition at temperatures below its calorimetric glass transition. The results, when taken together, indicate that the lowering of fictive temperature of the glass during aging results in a Q-species disproportionation of the type $Q^2 + Q^4 \rightarrow 2Q^3$, and all three relaxation processes are characterized by similar average timescales. Although these processes appear to be causally related, the non-exponential nature of Q-speciation and volume relaxation is found to be significantly different, which is hypothesized to be a manifestation of the corresponding differences in their associated length scales.

Acknowledgements

I would like to express my sincere gratitude to my advisor, Professor Sabyasachi Sen, whose unwavering patience knows no bounds. I am deeply thankful that he was supportive through the entire process of this longer-than-typical thesis development. He has truly been a great teacher. I sincerely feel that I was able to learn the process of research through his pointed questions and suggestions. Thank you, Professor Sen. I would also like to thank Professor Subhash Risbud and Professor Ricardo Castro for serving on my thesis committee.

Thank you to my dear friend and esteemed colleague, Dr. Srikanth Varanasi, whose enduring impatience served as extra motivation in the journey to completion of this thesis. He has been a great mentor and was always available if I needed encouragement or advice. I would also like to express my gratitude to NSG and Pilkington North America. Through my 15-year career with NSG I have worked with many capable, wonderful people who have encouraged me and given me opportunities to grow in my career. This thesis is one step in that process, and I appreciate the support I've gotten to that end.

Finally, I would like to thank my family. My spouse, Chris Spivey, whose support has been solid and persistent over the last eight years. My amazing daughters, Azalea and Claire, who have given me added purpose and are always there as a reminder of what is important. My parents, Denise and John, whose guidance has helped me navigate the winding path that has gotten me to this point. Thank you to all.

Table of Contents

List of Figures

List of Tables

1. Introduction and motivation

Glasses were first created by man over 4000 years ago, perhaps arising from the glazing process of earthenware and resulting in the production of small glass beads. More definitive evidence of glassmaking comes from the late Bronze age when small, colourful but opaque glasses were used to make small vials or vessels that exploited the nonporous and inert properties of the material. Subsequent advancement in glass technology resulted in transparent materials, which also incorporated chemical control of color by incorporating, for example MnO, to reduce Fe^{3+} to Fe^{2+} thereby minimizing the colorant effect of iron. The technique of glass blowing led to easier and therefore cheaper production of glass and was adopted for production of larger pieces. The use of glass then progressed to scientific products including glassware, lenses etc. [1]. The transparency and durability of glass are heavily utilized in contemporary applications ranging from containers, windows, lighting, reinforcement fibers, optical telecommunication fibers, electronic displays, lasers, insulation, all the way to nuclear waste encapsulation and art. The oxides make up over 95% of the glass products in current commercial applications. A large portion of these are silicates, of which particularly common are the soda-lime (Na, Ca) silicates due to their low cost, relatively high durability, and high transmission in the visible wavelength range [2].

As the applications of glass become more technologically advanced, the processing requirements become more stringent, which requires a deeper understanding of the fundamentals of the glassy state. One example of the more exacting requirements in a modern application is the use of alumino-silicate glasses as substrates for thin-film-transistors (TFT) in liquid-crystal displays. The dimensional stability requirements for the glass substrate in this application are very precise, on the order of <20ppm for poly-Si applications [3]. Thus, it is critical to understand the behaviour of the glass substrate at the high processing temperatures required for TFT production so that the thermal dimensional stability can be controlled. One

method of improving the dimensional stability at processing temperatures is by annealing prior to processing, which allows the glass to undergo structural relaxation and be more stable when the temperature is increased for processing.

Glass itself can be described by the recent definition presented by Zanotto and Mauro as "a nonequilibrium, non-crystalline condensed state of matter that exhibits a glass transition. The structure of glasses is similar to that of their parent supercooled liquids (SCL), and they spontaneously relax toward the SCL state. Their ultimate fate, in the limit of infinite time, is to crystallize [4]." This definition hints at the principles at play when examining the thermal behavior of glass. It addresses the structure of the glass being like that of a liquid, so although there is some short-range order, it lacks any long-range order that is characteristic of a crystalline material. This definition also puts forth the key principle of relaxation, which describes the behavior of the supercooled liquid in the glass transition range. The fact that a glass spontaneously relaxes towards the SCL state is what makes the concept of the thermal history of the glass an important one. Unlike crystalline matter, glasses are in metastable equilibrium and their properties are dependent on its thermal history. Understanding relaxation behaviour in the glass transition range can be of utmost importance in technical applications.

This dissertation reports the results of an investigation into the relaxation behavior of a soda-lime silicate float glass upon annealing below its glass transition temperature T_g i.e. aging. The relaxation of the volume and the short-range structure of the glass are followed using density and Raman spectroscopic measurements, respectively, and is compared with the shear relaxation timescale. First some theoretical background is presented to give context to the subsequent sections, including an overview of silicate glass structure, specifically SiO_2 and alkali-alkaline earth silicates as pertinent to the material studied here. A brief background of Raman spectroscopy fundamentals along with its application to soda lime silicates is presented. The next section gives a brief overview of the general relaxation behaviour as expected and

understood in the glass transition range, including a description of shear relaxation. Then the following sections present the experimental results obtained in the present study and discuss its fundamental implications on our current understanding of the aging behavior in network glasses.

2. Background

2.1. Structure of silicate glasses

Glass lacks the symmetry and long-range periodicity of a crystal and has a structure similar to liquids, both in its isotropic nature and in the variation in bond angles and lengths. These variations lead to a somewhat definitive order at the short-range i.e. at the nearest-neighbor length scale (up to ~ 2 Å) that becomes increasingly less precise as the structure is examined at longer length scales through the intermediate and the long-range. Structural attributes at the intermediate range include connectivity between the constituent structural moieties, while long range order includes structural characteristics such as density and composition fluctuations.

Silica (SiO_2) is considered the archetypal network glass, which is characterized by a fully connected, three-dimensionally continuous random network consisting of corner sharing SiO_4 tetrahedra. Figure 1 shows a two-dimensional representation of this network. The oxygen atoms that connect pairs of tetrahedra are known as bridging oxygen (BO).

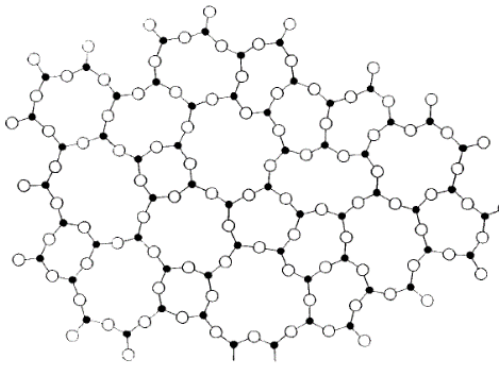

Figure 1: 2-D representation of the Continuous Random Network model of SiO_2 showing SiO4 tetrahedra connected through bridging oxygens to neighboring tetrahedra [5].

The radial distribution function (RDF) of silica as determined from neutron diffraction data (Figure 2A) contains information about the short, medium, and long-range order [6]. The first two peaks of the RDF represent the Si-O bond distance of ~ 1.608 ± 0.004 Å and an O-O distance of ~ 2.626 ± 0.006 Å. The O-Si-O bond angle is denoted by a distribution with a maximum at ~ 109.7° and Si-O-Si bond angle maximum is ~149°. The area under the first peak yields a Si-O coordination number of approximately 4 and an O-Si coordination of about 2.

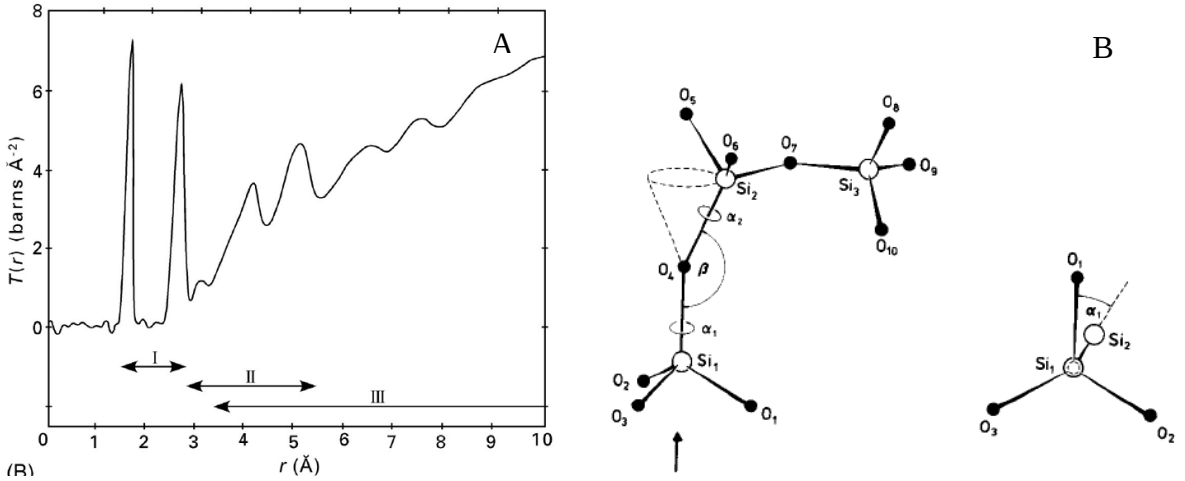

Figure 2: (A) RDF showing short, intermediate, long range order of SiO2 glass, denoted by roman numerals I, II and III, respectively. (B) Diagram of the basic structural unit of SiO2 [6].

The building block of the SiO_2 network, the SiO_4 tetrahedra (Figure 2B), then must connect to other tetrahedra in a non-periodic way that reflects the distribution of bond angles. This structural attribute is captured in the ring statistics, which describe how many SiO_4 tetrahedra are connected typically in a closed loop forming the shortest path. Multiple computer simulations show a combination of mostly 4- through 8-membered rings. Barmes *et al*. showed a distribution around 6-membered rings [7] which are the size of rings in β-crystobalite, a crystalline SiO_2 polymorph shown to be structurally the most similar to molten SiO_2 [1]. There are also a small number of 3-membered rings and puckered 4-membered rings, which have been observed in the Raman spectra (see below) [8,9].

The fully connected silica network can be modified upon the addition of "network modifier" oxides. Alkali and alkaline-earth ions are considered to be the typical network modifiers due to their role in interrupting the network connectivity. As alkali and alkaline earth elements are added, the network connectivity decreases with the introduction of non-bridging oxygen atoms (NBO), which are bonded to only one Si atoms and one or more modifier cations. Such a "modified random network" (MRN) is shown in Figure 3. Upon modification the Si-O-Si linkages of the silica network break and each alkali ion introduces one NBO and each alkaline-earth ion introduce two NBOs via the structural reactions: Si-O-Si +R_2O = 2 (Si-NBO---R) and Si-O-Si + RO = 2(Si-NBO)---R, respectively. The introduction of modifiers significantly alters the physical properties of the glass/liquid including viscosity, glass transition temperature, and ionic conductivity.

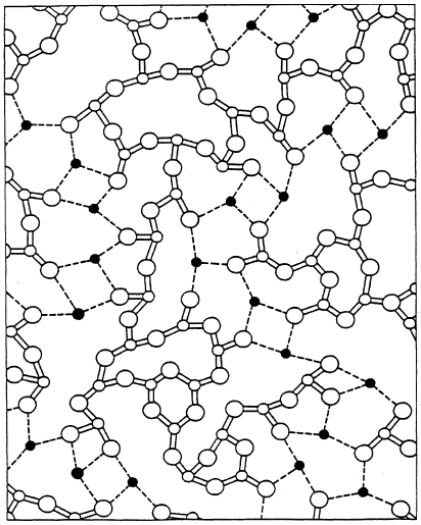

Figure 3: Depiction of Modified Random Network representing structure of a modified silicate glass [10]. Large and small open circles represent O and Si atoms, respectively, while filled circles represent modifier ions.

The spatial distribution of NBOs is an important characteristic in the description of the intermediate-range structure of a silicate glass. Nomenclature from ^{29}Si nuclear magnetic resonance (NMR) spectroscopy is typically used to describe the different SiO_4 tetrahedral units in silicates with varying number of NBOs by denoting the units as Q^n species, where n corresponds to the number of BO atoms on a given tetrahedra. ^{29}Si magic-angle-spinning (MAS) NMR spectroscopy has been very effective in measuring the types and relative fractions of Q^n species present in a given composition of glass. Representative ^{29}Si MAS NMR spectra for Na_2O-Si_2O glasses are shown in figure 4A with the relative abundance of each Q^n species for each composition in figure 4B [1, modified from 11]. It can be seen in this figure that at a given composition there is typically more than one Q^n species present, which has been corroborated by numerical modelling (Figure 4C).

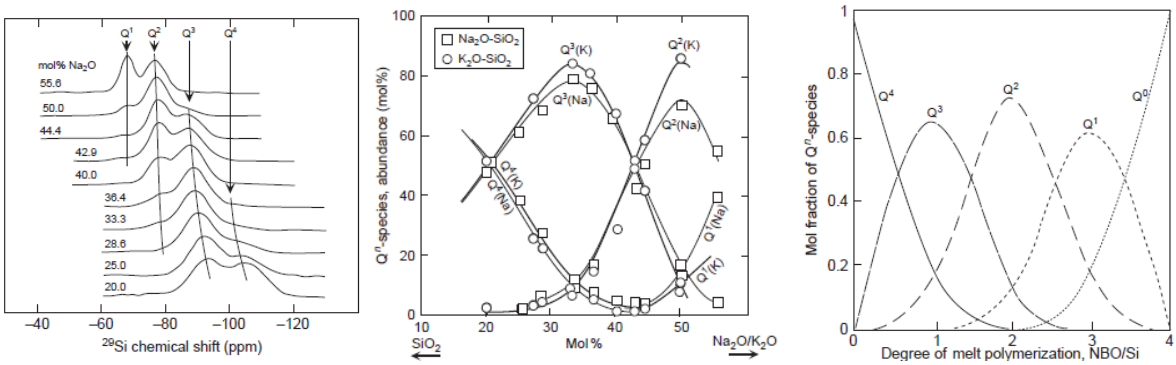

Figure 4: (A) 29Si NMR spectra of Na-silicate glasses denoting peak locations of various Qn species (B) Composition dependence of Qn species abundances in Na- (squares) and K- (circles) silicate glasses [1,11] (C) Numerical modelling of Qn speciation as a function of the degree of melt polymerization [12].

Composition, of course, is one of the main determinants of Q^n species abundances. As can be seen in Figure 4B the type of modifier cation can also influence the Q^n species abundance. While the total number of NBOs is fixed by the modifier content, the effect of the modifier type on the Q^n speciation can be described in the following disproportionation reaction: $2Q^n \leftrightarrow Q^{n-1} + Q^{n+1}$, where $1 \leq n \leq 3$, with the disproportionation reaction shifting to the right with increasing ionization potential of the modifier cation. Temperature and pressure also have an effect on the Q^n species abundance of a given composition [13-16]. Given difficulties of measurements on melts at high temperatures, it is common to quench a melt that has reached equilibrium at a high temperature and then measure the resultant glass at room temperature as the structure is frozen in at the glass transition. This method and using NMR measurements confirmed a shift to the right of the disproportionation reaction with increasing temperature [13]. In situ high-temperature Raman spectroscopy of silicate melts has confirmed this trend that is consistent with increasing configurational entropy with temperature (Figure 5). It is this change in Q^n speciation with temperature that is examined in the present study to determine structural relaxation behavior below T_g for a Na-Ca- silicate glass (see below).

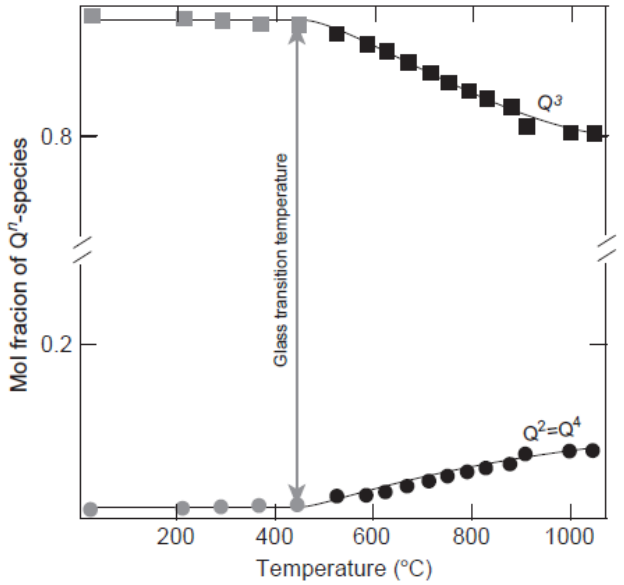

Figure 5: Q^n species dependence on temperature via in-situ Raman spectroscopic measurements in an alkali silicate melt [1, 14].

2.2. Raman spectroscopy of silicate glasses - background

In the present study we use Raman spectroscopy as the principal technique to investigate the structure of the glass under investigation and its evolution with temperature and time. Therefore, here we present a short introduction to the basic principles of this vibrational spectroscopic technique in relation to its application on silicate glasses. Vibrational spectroscopy is a well-established method of characterizing molecular structure in a material by describing the interaction of its vibrational motions with light. These vibrational motions are created by atoms executing small, periodic displacements about their equilibrium positions. The vibrational spectrum is determined by the nature of the atoms present, their relative arrangement, and the forces between them. This makes it possible to glean information regarding the local structure of a material from the spectra. Raman spectroscopy uses monochromatic light typically at a wavelength in the visible or near-infrared region directed onto a sample. Light in this region has a much higher frequency than vibrational frequencies and the oscillating electric field created by the light will cause electrons to displace relative to

their nuclear positions which will result in an induced dipole moment, $\vec{\mu}_{ind}$. The magnitude of the induced dipole is dependent on the electric field strength, $\vec{E}$, and the molecular polarizability, α, through the Equation 1.

$$\vec{\mu}_{ind} = \alpha\vec{E} \quad \text{[Eq. 1]}$$

The induced dipole moment is time dependent because of the electric field of the incident light is oscillating at a certain frequency, ν^*, and is described by Equation 2.

$$\vec{\mu}_{ind}(t) = \alpha\vec{E}(t) = \alpha E_o cos2\pi\upsilon^* t \quad \text{[Eq. 2]}$$

The polarizability varies with vibrational displacements, q_i, at any vibrational frequency, υ_i. This time dependence is described by expanding α in a Taylor series about its equilibrium position as shown in Equation 3.

$$\alpha(t) = \alpha_o + \left(\frac{d\alpha}{dq_i}\right)_o q_i cos2\pi\nu_i t + \cdots. \quad \text{[Eq. 3]}$$

Including the time dependency of the electric field, the polarizability, $\vec{\mu}_{ind}(t)$ can be decribed by Equation 4.

$$\vec{\mu}_{ind}(t) = \alpha_o E_o cos2\pi\upsilon^* t + \frac{1}{2}\left(\frac{d\alpha}{dq_i}\right)_o q_i E_o cos2\pi(\nu^* + \nu_i)t$$

$$+ \frac{1}{2}\left(\frac{d\alpha}{dq_i}\right)_o q_i E_o cos2\pi(\nu^* - \nu_i)t \quad \text{[Eq. 4]}$$

This results in light re-emitted at the incident wavelength, ν^*, known as Rayleigh scattering, and also at the shifted wavelengths $\nu^* - \nu_i$ and $\nu^* + \nu_i$, known as Stokes and anti-Stokes scattering, respectively [18].

An energy transfer model can be used to describe Raman spectroscopy as shown in Figure 6 [19]. The monochromatic incident light has an energy $E_o = h\nu^*$ where h is Planck's constant and ν^* is the light frequency. For a molecule in its ground vibrational state, v=0, the incident energy can interact with the electronic wavefunction of the molecule taking it to a virtual state that then will immediately decay. If it decays back to the ground state, then the energy emitted

will be the same as the incident energy and Rayleigh scattering has occurred. If the molecule decays back to an excited vibrational state, v=1, the energy emitted will be slightly lower than the incident energy, equal to $E_o - h\nu_i$, and Stokes Scattering has occurred. If the molecule starts in the excited vibrational state and then decays to the ground state, the energy emitted will be greater than the incident energy and equal to $E_o + h\nu_i$, and anti-Stokes scattering has occurred.

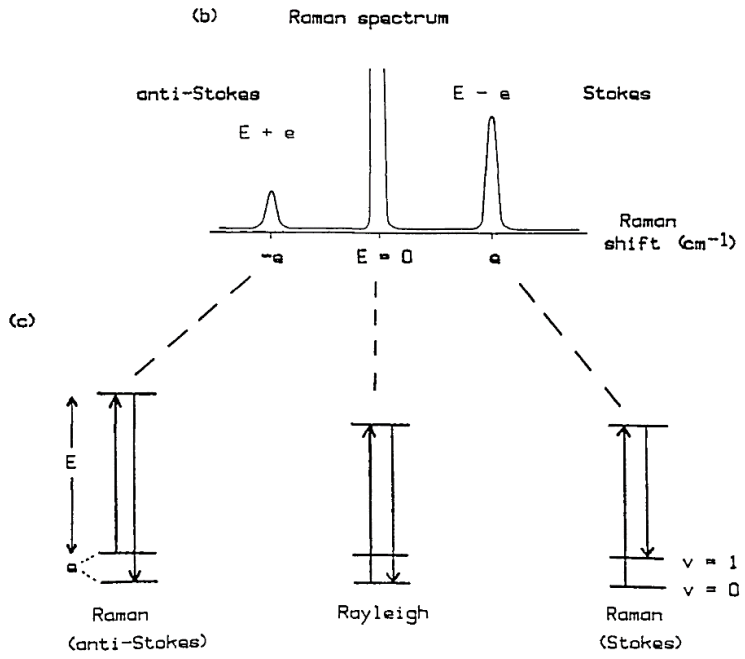

Figure 6: Diagram of energy transfer model of Raman Spectroscopy, from [19]

The structural assignments of the peaks/bands in the Raman spectra of binary alkaline and alkaline-earth silicate glasses has been carried out in previous studies in the literature by both comparing to crystals at similar compositions and by investigating a range of compositions usually starting with vitreous silica and then gradually increasing the modifier content [20-22]. Examples of these methodologies are shown in Figure 7A-B.

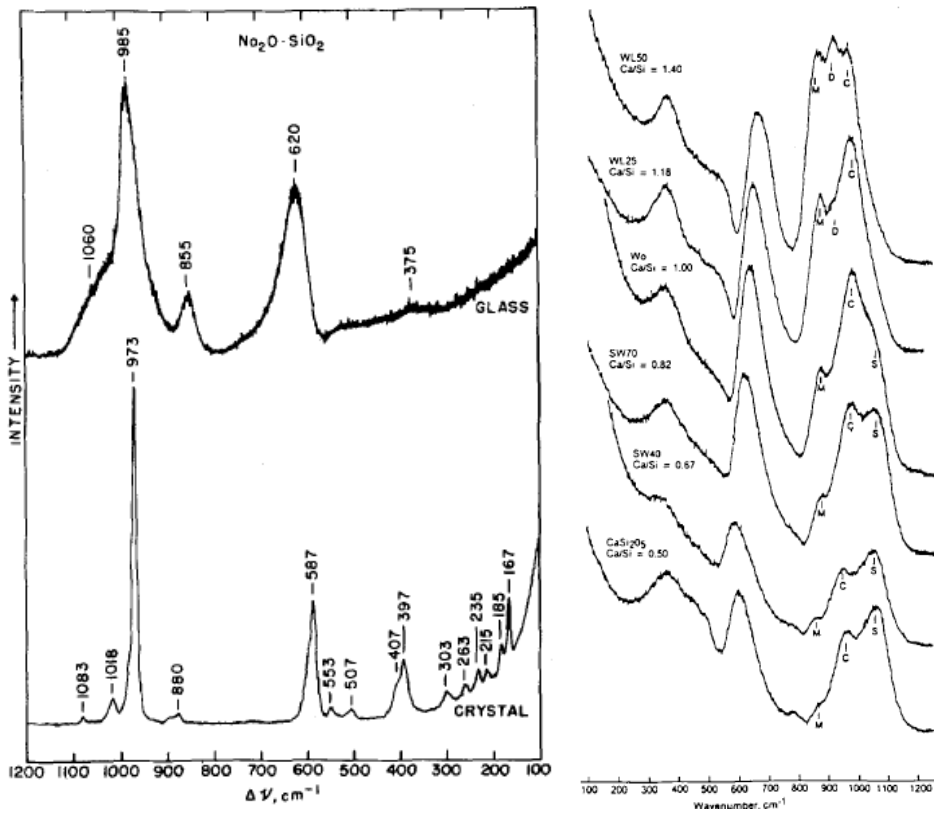

Figure 7: (A) Raman spectra of glass and crystal of Na2O-SiO2 , showing peaks in similar locations indicating the glass structure likely has some basis in the Si2O6 units (Q2) characteristic of the chain structure of the metasilicate crystal. This is an example of determining peak assignments by comparing Raman spectra of glass to that of crystal of the same composition [20]. (B) Raman spectra of glasses along the SiO2-CaO join with S, C, D, and M denoting sheet, chain, dimer, and monomer, or Q3, Q2, Q1, and Q0, respectively. As modifier content is increased, peaks representing the depolymerized units appear and increase in intensity. This is an example of determining peak assignments by varying composition from low NBO number to higher NBO number. [21]

The Raman spectra of silicate glasses can be split into three regions, the high frequency range (900-1200 cm^{-1}), the mid frequency range (700-800 cm^{-1}), and the low frequency range (400-700 cm^{-1}). The Raman spectrum of pure SiO_2, see Figure 8 [23], shows weak bands in the high frequency region at 1050 cm^{-1} and 1200 cm^{-1}. These are typically attributed to longitudinal-transverse (LO-TO) splitting of the optical mode of Si-O stretching vibration of the linked SiO_4 tetrahedra i.e. the Q^4 species. In the mid frequency range the band at 800 cm^{-1} is attributed to motion of Si atoms against their tetrahedral oxygen cage, with little associated

oxygen movement. The low frequency range shows one broad band at 430 cm^{-1} and two sharp bands at, 492 cm^{-1} and 606 cm^{-1}. The 430 cm^{-1} band is associated with oxygen motion in Si-O-Si bending, its width being dependent on the distribution of Si-O-Si angles within the SiO_2 network structure. On the other hand, the sharp bands at 492 cm^{-1} and 606 cm^{-1} correspond to symmetric oxygen breathing vibrations of four- and three- membered siloxane rings existing as "defects" within the network structure [18].

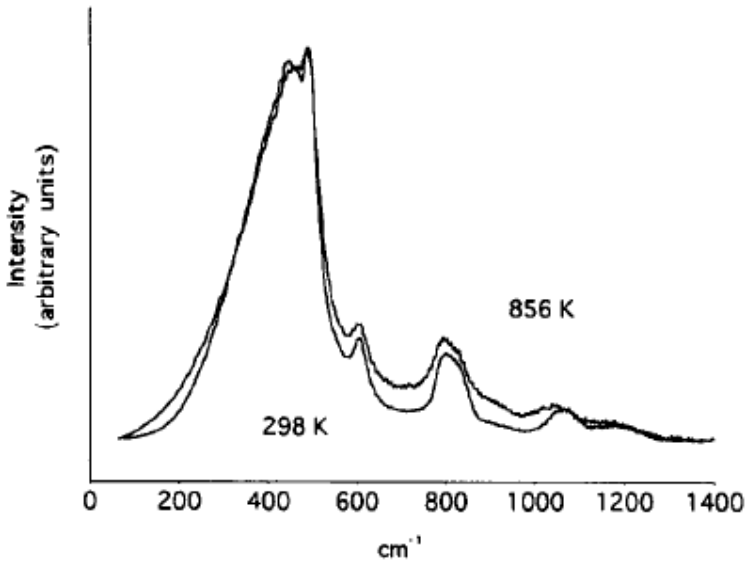

Figure 8: Raman spectra of SiO2 glass at different temperatures. The presence of bands at 430 cm^{-1}, 492 cm^{-1}, 606 cm^{-1}, 800 cm^{-1}, 1050 cm^{-1}, and 1200 cm^{-1} indicating structural units as discussed in the text [23]

Figure 9A shows another example of a series of Raman spectra of differing compositions. This series published by Fukumi *et al.* is of Na_2O-SiO_2 glasses with increasing Na_2O content and with the pure SiO_2 spectrum for comparison [24]. In the low frequency region, as SiO_2 content decreases the intensity of the 430 cm^{-1} band decreases, this supports the band being indicative of the SiO_4 tetrahedra network that is depolymerized as alkali content increases. As alkali or alkaline earth content increases, bands appear in the regions 520-600 cm^{-1}, 590-650 cm^{-1}, and

near 700 cm^{-1}, which possibly correspond to the same Si-O-Si bending modes of the Q^3, Q^2, and Q^1 species, respectively. The frequencies of the bands in the 400-700 cm^{-1} range seem to be sensitive to Si-O-Si bond angle where the peaks shift to higher frequency with lower expected bond angle. In the mid-frequency range, the 800 cm^{-1} band that is seen in pure SiO_2 tends to move towards 770 cm^{-1} and disappears below 60 mol% silica. [25]

In the high frequency region, the bands are assigned to symmetric Si-O stretching motions of the various Q^n species. The bands near 1100-1050 cm^{-1}, 1000-950 cm^{-1}, 900 cm^{-1}, and 850 cm^{-1} are attributed to Q^3, Q^2, Q^1, and Q^0 species, respectively [26]. It can be seen in Figure 9A that the peaks in this region are indeed shifting in a way to denote the increase of less polymerized Q^n species with increasing alkali content and are fairly well-resolved. Figure 9B shows decomposition analysis of the high frequency region of the Raman spectrum of a Na_2O-$4SiO_2$ glass at 1457°C. The 950 cm^{-1} and the 1100 cm^{-1} bands are clearly representative of Q^2 and Q^3 units, respectively. The assignment of the weaker bands at 1050 cm^{-1} and 1150 cm^{-1} are less clear. The 1150 cm^{-1} band is typically attributed to the Si-O stretching of Q^4 species. The 1050 cm^{-1} band has been attributed to Si-O stretching with a bridging oxygen, but not necessarily of the Q^4 species or, alternatively as a vibration in structural units associated with the metal cation [14, 24, 27]. In the present study we employ similar Raman band decomposition analysis to investigate the structural evolution of the Na-Ca- silicate glass under investigation with temperature and time during annealing.

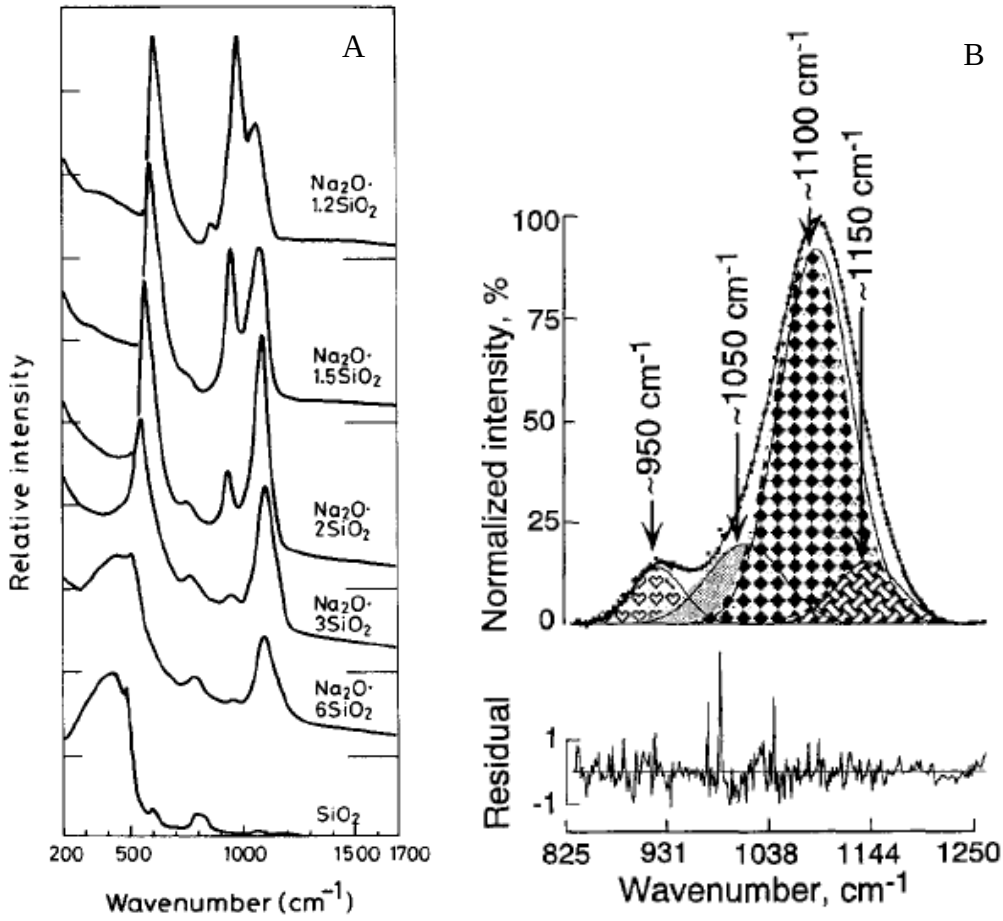

Figure 9: (A) Raman spectra of glass along the Na2O - SiO2 join. Peaks discussed in text [24]. (B) Example deconvolution of high frequency envelope by curve fitting on a spectra of Na2O-4SiO2 at 1457° C [14]

2.3. Relaxation in glasses

2.3.1. Description of relaxation behavior

The description of the thermodynamic state of a glass requires not only temperature T and pressure P, but also a parameter denoting the average structure of the liquid. This average structure is sometimes described in terms of the fictive temperature T_f of the glass, which depends critically on the thermal history of its parent liquid in the glass transition range. As the temperature of the system decreases, the viscosity of glass-forming liquids increases such that at sufficient undercooling the supercooled liquid cannot reach equilibrium on an experimental timescale. This causes the liquid structure to be frozen in at the glass transition.

The dependence of the glass transition temperature, Tg, on the cooling rate is evidence that the glass transition is predominantly kinetic in nature. This phenomenon is shown in Figure 10 as a plot of enthalpy H vs T of a glass-forming liquid being cooled and heated through the glass transition range at two different rates. A liquid cooled at a faster heating rate will drop out of equilibrium at a higher temperature compared to a liquid cooled at a slower rate [28]. Also, to note in Figure 10 is that upon reheating the observed property exhibits a hysteresis due to the kinetics of the relaxation process. The bottom diagram shows an example of the derivative of the property, in this case heat capacity.

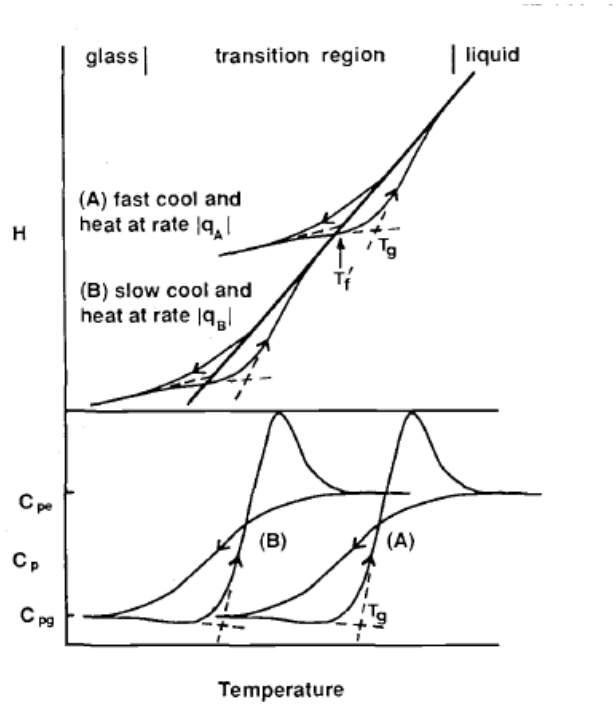

Figure 10: Top plot showing effect of cooling rate on Tg, Tf, and H . Bottom plot showing Cp upon heating as a determination of Tg [28].

Relaxation is the process of return or recovery of a glass or supercooled liquid to equilibrium following a perturbation away from its equilibrium state. In its simplest form relaxation can be described as a first order kinetic process with a rate constant, k such that the

rate of recovery of a property with its value at time *t* being ρ_t is proportional to the degree of deviation from the equilibrium value ρ_e, which can be expressed as:

$$\frac{d(\rho_t-\rho_e)}{dt} = -k(\rho_t - \rho_e) \quad \text{[Eq. 5]}$$

Integration of equation 5 yields the relaxation function $\phi(t)$ (Eq. 6). The inverse of the rate constant (-1/k) corresponds to the relaxation time t. The relaxation function $\phi(t)$ = 1 at t = 0 and reaches 0 at times significantly longer (t > 5*τ) than the relaxation time. Over limited temperature ranges the temperature dependence of τ can be described by an Arrhenius expression (Eq. 7), where ΔH* is the activation energy and R is the gas constant. As T decreases t increases, leading to exponentially longer relaxation times as temperature is lowered. At lower temperatures and for fragile glass formers the relaxation time becomes increasingly non-Arrhenius.

$$\phi(t) = \frac{(\rho_t - \rho_e)}{(\rho_o - \rho_e)} = \exp(-kt) = \exp\left(\frac{-t}{\tau}\right) \quad \text{[Eq. 6]}$$

$$\tau = A \exp\left(\frac{\Delta H^*}{RT}\right) \quad \text{[Eq. 7]}$$

Quantitatively, relaxation doesn't always follow the above linear description. An example of this is shown in Figure 11, where two glasses were equilibrated at different temperatures, one at 500°C and one at 565°C, and then both were allowed to relax at 530°C. The rate of relaxation is faster for the glass that was equilibrated at the higher temperature, i.e. had a higher fictive temperature T_f [28, 29]. This indicates that t is dependent on the structure of the glass or T_f. A common way of accounting for this dependence of τ on T_f is by using the Tool-Narayanaswamy (TN) equation as shown in Equation 8 below. In this equation *x* is the nonlinearity parameter and varies between 0 and 1. Relaxation becomes increasingly non-linear with small values of *x* and large departures in temperature from T_f. Small values of *x* indicate relaxation rates that are strongly dependent on structure.

$$\tau = \tau_o \exp\left[\frac{x\Delta H^*}{RT} + \frac{(1-x)\Delta H^*}{RT_f}\right] \quad \text{[Eq. 8]}$$

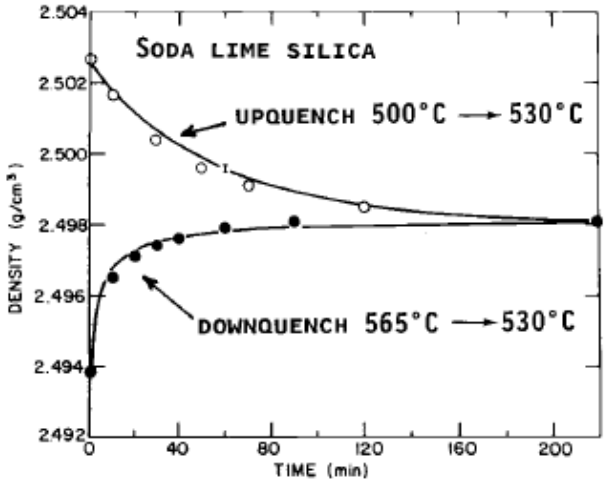

Figure 11: Density relaxation of samples at a temperature above or below Tf showing that linear relaxation does not always fit and is dependent on Tf. The sample relaxing down (i.e. with the higher fictive temperature) relaxes more quickly than the sample with lower fictive temperature [28].

The dependence of τ on the structure is also embodied in the Adam-Gibbs formalism, which incorporates the configurational entropy S_c of the supercooled liquid as a temperature dependent quantity that is responsible for various degrees of non-Arrhenius temperature dependence of τ (Eqs. 9,10). In the following equations B is a constant, ΔC_p is the difference between the heat capacities of the liquid and the glass across T_g, and T_k is the Kauzmann temperature, which is the temperature where, compared to the crystal, the excess entropy of the glass is zero.

$$\tau = \tau_o \exp\left[\frac{B}{TS_c(T_f)}\right] \quad \text{[Eq. 9]}$$

$$S_c(T_f) = \Delta C_p \ln\left({}^{T}/_{T_K}\right) \quad \text{[Eq. 10]}$$

Not only does the relaxation behaviour deviate from a purely linear equation, it also deviates from a true exponential function. The relaxation function in this general case can be

described using a stretched exponential, which is commonly known as the Kolrausch-Williams-Watts (KWW) function:

$$\Phi(t) = \exp - \left(\frac{t}{\tau}\right)^{\beta} \quad \text{[Eq. 11]}$$

In this equation t is the experimental time, β is the KWW exponent, and t is the characteristic relaxation time. The KWW function is used as a way of describing the average relaxation time in a system that is characterized by heterogeneous dynamics with the coexistence of a range of relaxation times. The exponent β ranges between 0 and 1, and as β approaches 0 the relaxation deviates more from the true exponential, which indicates an increasingly broad distribution of relaxation times [29]. This broad range in relaxation times may be the result of spatial and/or temporal heterogeneity in the dynamical events responsible for the relaxation. [28,29]. In this scenario the individual dynamical events are exponential but with different time constants such that the ensemble average leads to a stretched exponential bulk relaxation. An alternate scenario is a hierarchical relaxation process, which leads to individual dynamical events that are inherently non-exponential. Moreover, different variables such as enthalpy and density may be characterized by different values of τ and β [30]. When the Kohlrausch exponent, β, and the characteristic relaxation time, τ, have been defined, then the average relaxation time, <τ>, is described by Equation 12 where Γ is the gamma function [28].

$$< \tau > = \left(\frac{\tau}{\beta}\right) \Gamma \left(\frac{1}{\beta}\right) \quad \text{[Eq. 12]}$$

2.3.2. Shear Relaxation and the Maxwell relation

Different properties, including viscosity, volume and structure, have been shown to have comparable relaxation rates in silicates. [1, 28, 31] This makes the Maxwell model a good approximate estimate of relaxation time of multiple properties based on viscosity [1]. At its base the Maxwell model considers a viscoelastic material as an equivalent to a spring and

dashpot in series, meaning an applied stress first results in an elastic strain, which would recover if released, then followed by a viscous deformation which would not recover.

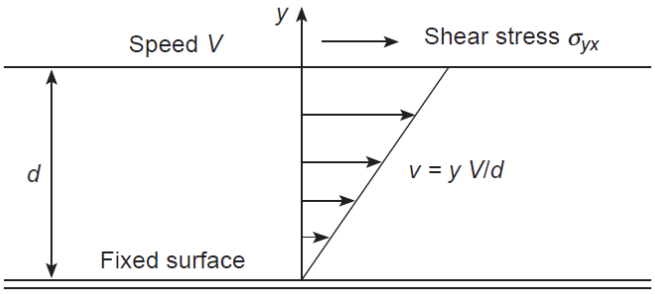

Figure 12: Schematic of velocity gradients in a liquid between two infinite planes [1].

This can be understood by first considering flow in a liquid as depicted in Figure 12. Shear stresses in liquids result in velocity gradients perpendicular to the flow direction due to the interatomic forces. The shear stress in a sample, σ, can be defined for a homogeneous relative strain (Equation 13).

$$\sigma = \eta \, {\partial \varepsilon}/{\partial t} \quad \text{[Eq. 13]}$$

Where η is the shear viscosity and ${\partial \varepsilon}/{\partial t}$ is the strain rate. A fluid is Newtonian if viscosity is independent of the stress and strain rate. As glass-forming liquids approach Tg their behavior becomes increasingly viscoelastic, meaning the elastic component becomes more and more important. The stress, σ, from the elastic component can be described by Hooke's law (Equation 14).

$$\sigma = G_\infty \varepsilon \quad \text{[Eq. 14]}$$

where G_∞ is the glassy shear modulus plateau value at very high frequency and ε is the strain. Therefore, the elastic strain rate can be described by Equation 15.

$$d\sigma/dt = G_\infty \, d\varepsilon/dt \quad \text{[Eq. 15]}$$

In addition to the elastic deformation, represented by the spring, is the viscous deformation, represented by the dashpot, that results in relaxation of the stress built up through the straining

of bond lengths and angles. This stress diminishes in time while maintaining the initial elastic deformation. Assuming the rate of relaxation is proportional to the value of the stress, Equation 15 can be written as Equation 16.

$d\sigma/dt = G_\infty \, d\varepsilon/dt - \sigma/\tau$ [Eq. 16]

Where τ is the stress relaxation time, also known as the Maxwell relaxation time, and describes the timescale of this process. When stresses are applied at low frequencies, dσ/dt becomes small and the equation, along with Equation 13, can be written as:

$\eta = G_\infty \tau$ [Eq. 17]

Using this equation, the shear relaxation time can be calculated if the viscosity is known. In practice, stress relaxation times are very similar to structural relaxation times and are used synonymously in literature [1]. This allows for the calculation of the temperature dependence of the structural relaxation time as long as the viscosity-temperature relationship is known, and the shear modulus is estimated within a factor of two. [31]. The shear modulus can be considered approximately constant over large ranges of composition and temperature, especially as compared to the variation of viscosity over the same ranges. Thus, G_∞ can be approximated to be ~ 30 GPa for all silicate glass-forming compositions [32]

2.3.3. Correlation between Structural and Shear Relaxation

Structural and shear relaxation times are frequently taken to be equivalent in silicate glasses and melts. Some of the evidence supporting this is summarized well by Dingwell [31] including a comparison between the longitudinal viscosity and the shear viscosity (Figure 13A) showing the expected relationship if volume viscosity was equal to shear viscosity, indicating equivalence between these two relaxation times. The demonstration of constant viscosity at a consistently defined calorimetric (or dilatometric) glass transition temperature for many different glass formers, as shown in Figure 13B, implies that the shear relaxation (which is

proportional to viscosity through the Maxwell relation), is closely related to the enthalpy and volume relaxation time [32]. It has also been shown in various studies, as compiled by Moynihan [28], that the temperature dependence of structural relaxation and shear viscosity as indicated by activation enthalpies are identical within experimental error. This has led to structural and shear relaxation times to be taken as equivalent in silicates.

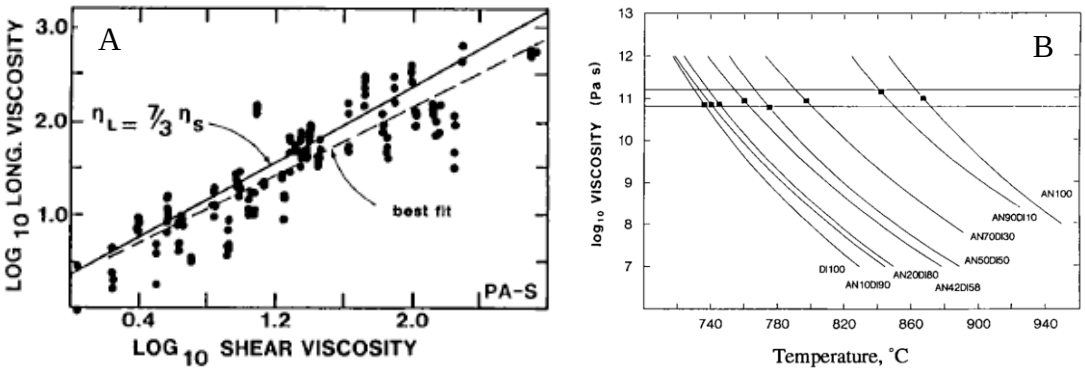

Figure 13: Indications of the equivalence of enthalpy, volume, and shear relaxation times. (A) The longitudinal viscosity vs shear viscosity plot exhibits the expected relationship if volume and shear viscosities were equivalent (solid line) (B) Plot of viscosity compared to temperature for different glass formers. Calorimetric T_g is denoted by the squares which are shown to be consistently at similar viscosities [32].

A recent publication by Lancelotti *et al*. calls this equivalence into question [33]. They measured the structural relaxation times of lead metasilicate glass during aging below T_g using refractive index as a proxy and compared these data to the calculated shear relaxation time. Their work showed that the shear relaxation time was significantly lower than the measured structural relaxation time. This discrepancy has in the past been attributed to experimental error, but they posit that the difference is real and that the shear relaxation time as calculated with Maxwell relaxation can only give a lower bound estimate of the structural relaxation time. The purpose of this study is to further explore this issue by investigating simultaneously the volume, structural and shear relaxation behaviour of a soda lime silicate glass during aging.

3. Experimental Details

3.1. Sample synthesis and chemical characterization

The Na-Ca-silicate glass used in this study was prepared at the Pilkington manufacturing plant at Lathrop, California, by the float process and is referred to as the NSG glass in the subsequent discussion. The Float process was invented by Pilkington in the 1950s as a method of floating glass on molten tin to create a product with very flat surfaces and uniform thickness. Float glass is a continuous process where the batch is fed into the front of the furnace and melted at around 1600°C. The melt proceeds through the furnace, cooling down to approximately 1100°C before pouring through the canal into the tin bath. In the tin bath the glass is formed to the proper width and slowly cooled to approximately 600°C so that it can be fed onto lehr rollers. The lehr rollers convey the glass ribbon from the exit of the tin bath through the annealing lehr. The thickness of the glass will depend on the speed that the lehr rollers are pulling the glass, a faster lehr speed will produce thinner glass. Thicknesses ranging from 1.3mm to 22mm are produced using the float method. Through the annealing lehr the glass is cooled in a controlled manner to eliminate permanent and temporary stress and delivered to the cutting and stacking area [34, 35]. A basic schematic of a float line is shown in Figure 14. A typical daily production yield of the float process is on the order of 500 tons per day. A small amount of glass from a production run of 2.2 mm clear-tint glass was acquired for use in this study.

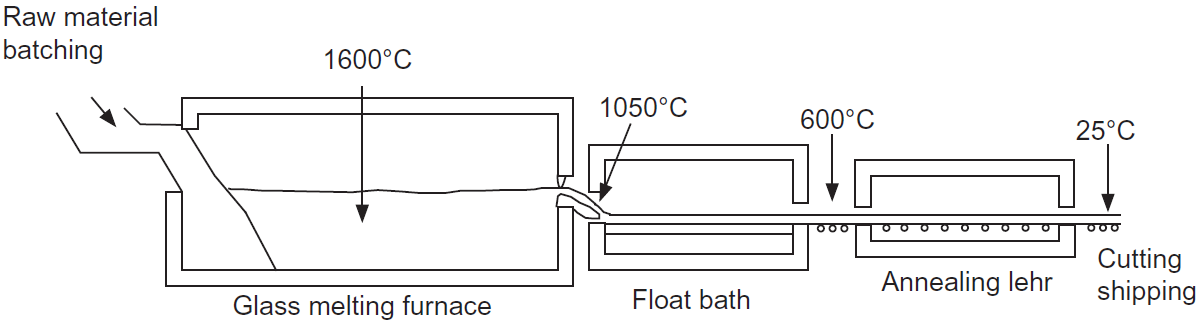

Figure 14: Schematic of float glass processing denoting temperatures throughout the process [35].

The chemical composition of the NSG glass was determined with an X-Ray Fluorescence (XRF) spectrometer (Philips PW-2424). A sample of approximately 25g was crushed using an agate mortar and pestle to smaller than 2mm fragments as confirmed by sieving. The crushed material was then ground in a ball mill (Retsch PM 200) and 8 grams of the ground material was mixed with 2 grams of wax powder. This mixture is then pressed into a pellet utilizing a SPEX hydraulic press activated to 27 tons of pressure. The prepared pellet is then inserted in the XRF spectrometer. The measured glass composition is detailed in Table 1 and is of a typical float glass composition.

The mol percent of the constituent network-forming and network-modifying oxides can be used to calculate the number of NBOs per SiO_4 tetrahedra and to determine the expected Q^n species. The minor constituents (Al_2O_3, Fe_2O_3, K_2O, TiO_2, and SO_3) were omitted from the NBO calculation. Each alkali ion (Na^+) then contributes 1 NBO and each alkaline earth ion (Ca^{2+}, Mg^{2+}) contributes 2 NBOs. For a total of 100 mol will result in 2*12.63 + 2*9.55 + 2*5.99 (Na^+ + Ca^{2+} + Mg^{2+}) = 56.3 mol NBOs. This number divided by the total number of tetrahedra (number of silicon atoms, 71.53 mol) gives the number of NBOs per tetrahedra. This calculates out to approximately 0.79 NBO/tetrahedra. Comparing this to figure 4C shows that the expected structural make up of this glass is a mix of Q^4, Q^3, and Q^2 species with Q^3 being the dominant species, followed by Q^4, and then Q^2 making up the smallest amount. As noted in the previous section the absolute number of Q^n species can vary with temperature and pressure

or with subsequent heating treatment that can alter the fictive temperature as conducted in this study.

3.2. Relaxation measurements

Viscosity of the supercooled NSG liquid was measured with a rotating cylinder viscometer in the 10^0 – 10^4 Pa.s range and with a beam bending viscometer in the 10^9 – 10^{13} Pa.s range. The samples of the NSG glass were approximately 2mm thick and were cut into squares 30 mm by 30 mm in size for volume relaxation experiments. Samples were annealed at either 500°C or 520°C for various lengths of time ranging between 1 hour and 40 hours. These temperatures were chosen because they are slightly below the glass transition temperature, but still within the glass transition range for relaxation. The density of the annealed samples was measured using the Archimedes' method. Each sample was measured in air and then in water. The temperature of the water was recorded so that an accurate water density could be used for further calculations. The density of the glass was then calculated using the Equation 17.

$$\text{Density}_{\text{glass}} = (\text{Weight}_{\text{air}} * \text{Density}_{\text{fluid}}) / (\text{Weight}_{\text{air}} - \text{Weight}_{\text{fluid}}) \quad \text{[Eq. 17]}$$

For each sample density measurement was repeated five times and the average values were used for further analysis. The Raman spectra of NSG glass samples annealed at 500°C were collected with a Bruker RFS 100/S FT Raman spectrometer equipped with a Nd:YAG laser operating at 1064 nm and a solid-state Ge detector in the frequency range of 0 – 1800 cm^{-1}. Each spectrum was an average of approximately 1024 scans.

Table 1: Composition of NSG glass as measured by XRF

Glass Composition		
Constituent	weight %	mol %
SiO2	73	71.53
Al2O3	0.17	0.10
Fe2O3	0.1	0.04
Na2O	13.3	12.63
K2O	0.03	0.02
CaO	9.1	9.55
MgO	4.1	5.99
TiO2	0.03	0.02
SO3	0.17	0.12

4. Results and Discussion

4.1. Shear Relaxation of NSG glass

Shear relaxation time for the NSG glass/melt was calculated using the measured viscosity and the Maxwell relation. The viscosity data for this glass composition in the temperature range of 550°C to 1445°C are given in Table 2. These viscosity data were fitted to the Mauro-Yue-Ellison-Gupta-Allan (MYEGA) model (Eq. 18) where η_o, K, and C are adjustable parameters [33, 36]:

$$\eta = \log_{10}\eta_o + \frac{K}{T}\exp\frac{C}{T} \quad \text{[Eq. 18]}$$

The MYEGA fit of the viscosity data is shown in Figure 15. This fit predicts viscosity at the annealing temperatures of 500°C and 520°C corresponding to the volume relaxation experiments to be ~$10^{16.5}$ Pa.s and $10^{15.2}$ Pa.s, respectively. Using the Maxwell relation and G_∞ ~ 30 GPa, this results in shear relaxation times t_{shear} of ~290 hours and ~15 hours at 500°C and

520°C, respectively. The glass transition temperature of silicate glasses corresponds to a viscosity of 10^{12} Pa.s. Therefore, the fictive temperature of the as-prepared glass sample can be taken to be ~ 583°C. Calculating the shear relaxation time gives a basis by which to compare structural relaxation measurements that were carried out on these samples through density and Raman spectroscopy measurements.

Table 2: Viscosity data of NSG melt

log η (Pa-s)	Temperature (C)
1	1445
1.5	1298
2	1192
3	1026
4	913
5	828
6.6	766
7	732
8	713
9	673
10	637
11	606
12	583
12.4	562
13.5	553

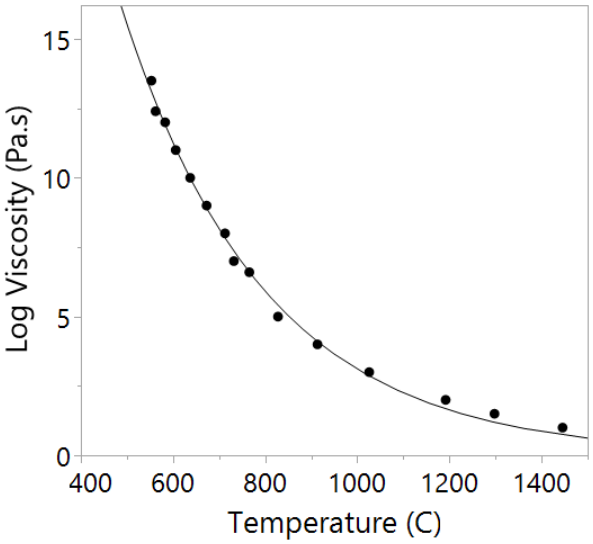

Figure 15: MYEGA fit of Log Viscosity vs Temperature plot for NSG melt

4.2. Volume Relaxation of NSG glass

The temporal evolution of the density of the NSG glass samples during annealing at 500°C and 520°C is shown in Figure 16. The observed increase in density with increasing annealing time at both temperatures is consistent with a glass that is equilibrating to a lower fictive temperature from the initial fictive temperature of 583°C.

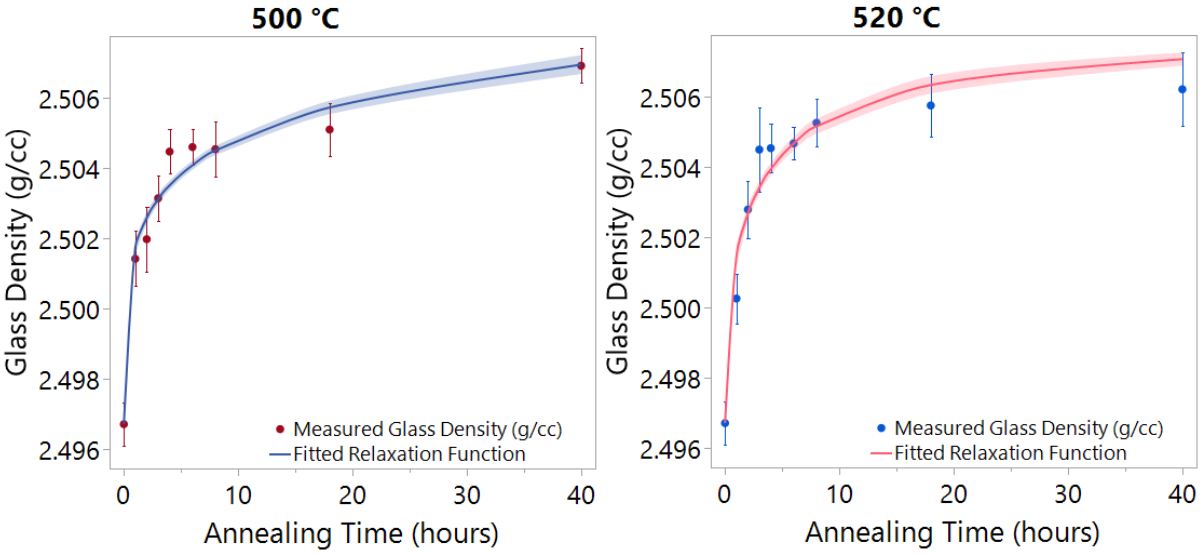

Figure 16: Variation of glass density with annealing time at annealing temperatures of 500°C (left) and 520°C (right). Density is increasing upon annealing indicating a move to lower fictive temperature. The error bars on the measured samples indicate the standard deviation of the measurements. The line represents the fit of the relaxation function. The shaded area represents the standard error of the fit.

As mentioned in the previous section, the expected shear relaxation timescales for the NSG glass at 500 and 520°C are on the order of ~ 290 and 15h, respectively. The temporal evolution of the density data in Fig. 16 was fitted to a stretched exponential relaxation function (Eq. 11) to obtain τ ~7.5h and β ~0.5 for annealing at 520°C, and τ ~295h and β ~0.3, for annealing at 500°C. Therefore, these density relaxation timescales correspond well with the expected shear relaxation times at these temperatures. The significant decrease in β with decreasing annealing temperature suggests a corresponding increase in the dynamical

heterogeneity i.e. in the width of the relaxation time distribution, which is a hallmark of glassy dynamics [37]. The equilibrium densities at as predicted from these fits are 2.5075 and 2.5115 g.cm^{-3}, respectively, at the fictive temperatures of 520 and 500°C. These density values, when combined with the measured density of 2.4967 g.cm^{-3} for the as-prepared glass with a fictive temperature of 583 °C, yield a linear variation in density with temperature (Fig. 17).

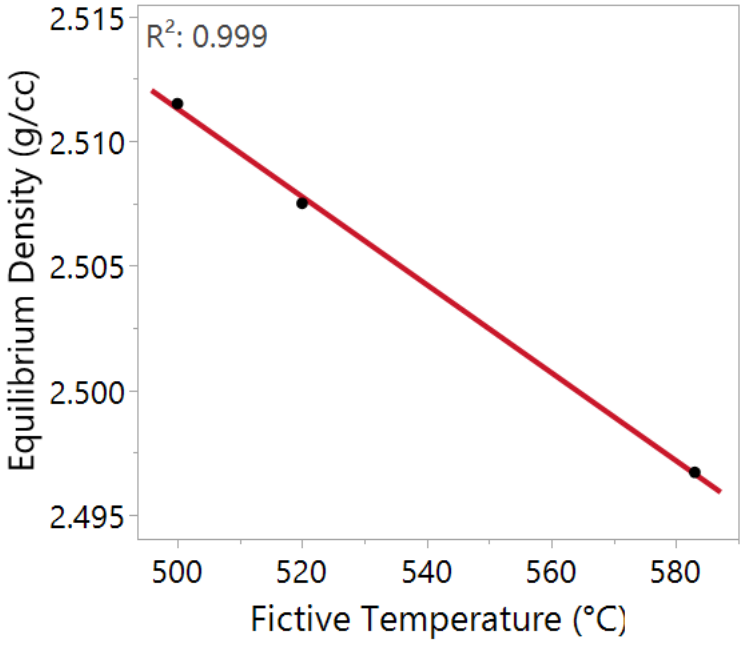

Figure 17: Equilibrium density vs fictive temperature of NSG glass. Straight line through the data points is a linear least-squares fit.

4.3. Raman spectroscopy and structural relaxation of NSG glass

The Raman spectra of NSG glass samples annealed at 500°C for various lengths of time are shown in Fig. 18. These spectra display the typical bands associated with an alkali-alkaline earth-silicate glass of this composition. The 450 cm^{-1} band is attributed to the Si-O-Si bending mode of the Q^4 species, while the 560 cm^{-1} band corresponds to the same mode for the Q^3 species. On the other hand, the 600 cm^{-1} band may be attributed it to either the Si-O-Si bending mode of the Q^2 species or the oxygen breathing vibration of three-membered siloxane rings. The 800 cm^{-1} band is attributed to the silicon motion against the tetrahedral oxygen cage. The

high frequency bands centered at ~ 950 cm^{-1} and 1100 cm^{-1}, correspond to symmetric Si-O stretching vibration modes of Q^2 and Q^3 species, respectively [14]. Detailed assignment of other bands under this high-frequency envelope is discussed in a separate section below.

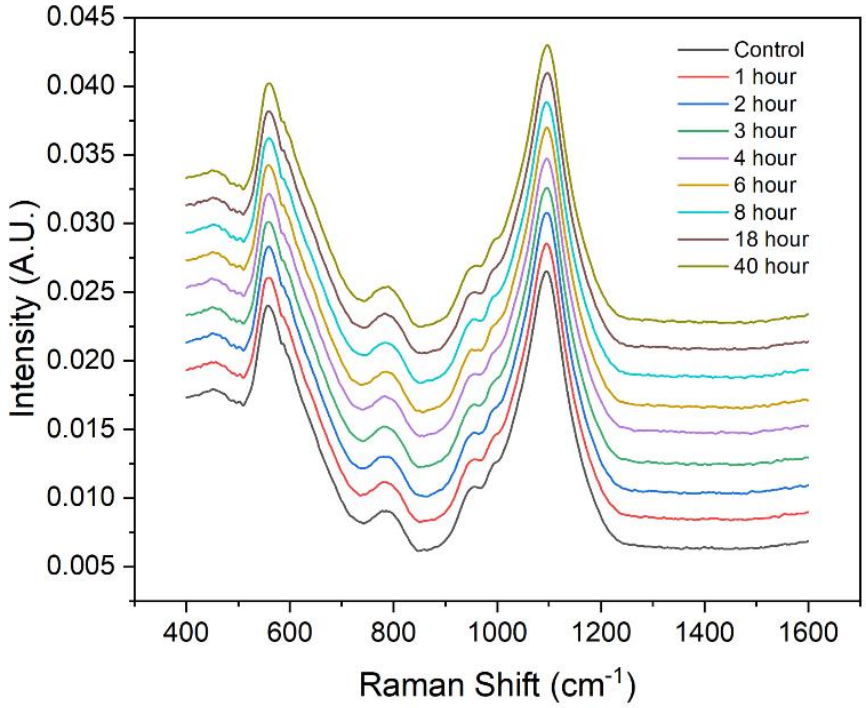

Figure 18: Raman spectra of NSG glass samples annealed at 500°C for various lengths of time.

As noted above, the change in density during relaxation is quite small, and therefore any structural change would be also expected to be subtle. This is the case as shown by the slight differences seen between the Raman spectra of these samples. The spectra are examined in more detail by splitting into low frequency (400 – 730 cm^{-1}) and high frequency (850 – 1200 cm^{-1}) regions. The normalized Raman spectra the low frequency range are shown in Figure 19A. The normalized intensity of the 450 cm^{-1} peak decreases with annealing time *t* and reaches a plateau for $t \geq 20$h, as shown in Figure 19B.

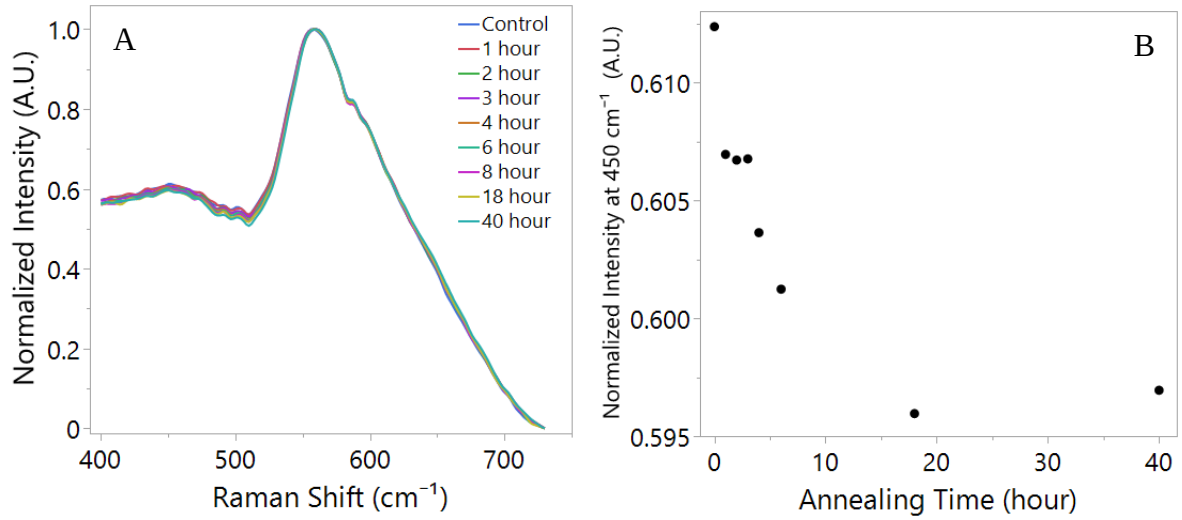

Figure 19: (A) Normalized Raman spectra of NSG glass samples annealed at 500 °C in the low frequency region (400 - 730 cm^{-1}). (B) Normalized intensity at 450 cm^{-1} as a function of annealing time.

Recently Deschamps *et al.* investigated the manifestation of the mechanical densification of window glass in the low-frequency Raman spectra [38]. These authors were able to find a Raman parameter that is linearly related to densification pressure and therefore to sample density. Deschamps et al. noted that after baseline subtraction and normalization of the Raman spectra in the region between 500 and 730 cm^{-1} that the shift of the peak maximum did not show a linear change with pressure but the intensity variation for the two peaks in the region, at 560 and 600 cm^{-1}, seemed to be linear. These authors proposed a Raman parameter, σ, as the frequency value where the integral fraction of the 500 to 730 cm^{-1} frequency region equals 0.5, described by the Equation 19 [38].

$$\frac{\int_{500}^{\sigma} I_{Raman}(\omega)d\omega}{\int_{500}^{730} I_{Raman}(\omega)d\omega} = \frac{1}{2} \qquad \text{[Eq. 19]}$$

To determine σ for the annealed NSG glass samples studied here, the integral fraction at each frequency was calculated for all spectra in Fig. 18 after baseline subtraction and normalization (Figure 20A,B). The frequency where the integral fraction is equal to 0.5 yields the value for σ. Figure 20C shows a close up of this region for all the spectra and the general increase in σ

as the annealing time increases. The variation of σ vs. the annealing time at 500°C is shown in Figure 20D, which shows strong similarity with that of the density of these samples and indeed these two quantities (σ and density) show excellent positive correlation (Fig. 21).

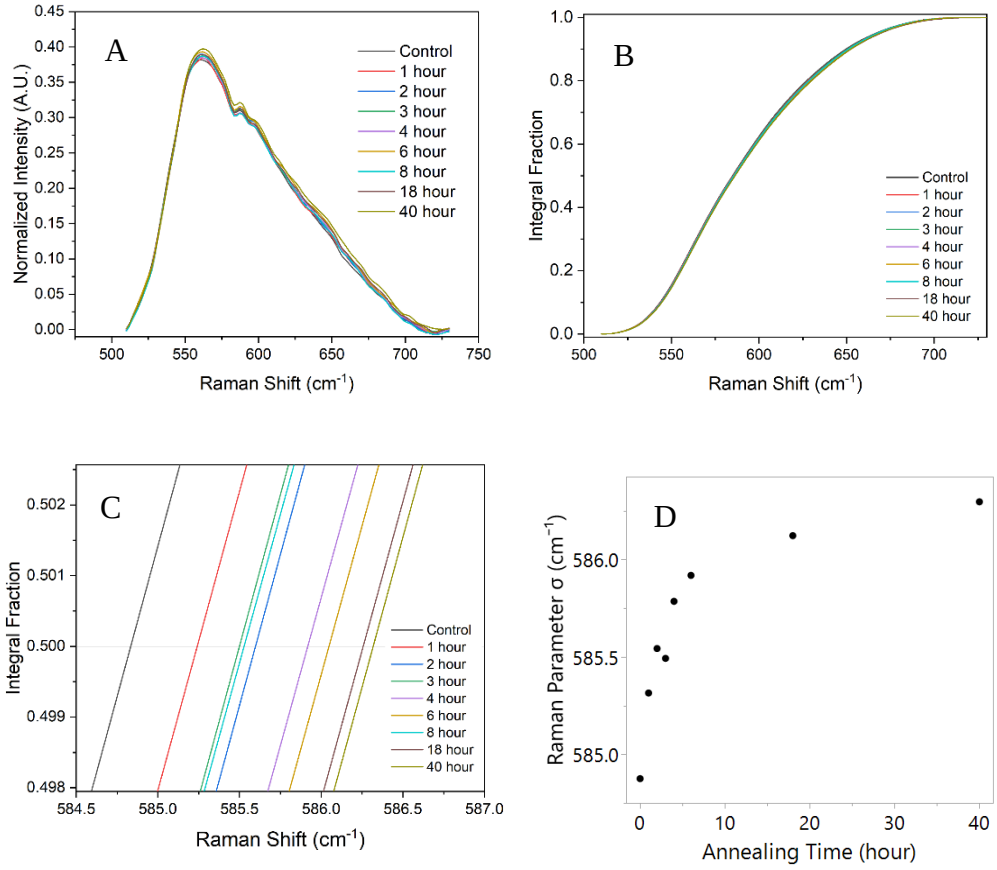

Figure 20: (A) 500cm^{-1} – 730cm^{-1} frequency region of Raman spectra after normalization and baseline subtraction, shown for all samples. (B) Integral fraction of the 500cm^{-1} – 730cm^{-1} frequency region of the normalized spectra from (A). (C) Magnified view of the integral fraction of all spectra with horizontal line showing location of σ where the integral fraction is 0.5. (D) Raman Parameter σ as a function of annealing time at 500 °C.

A simple linear fit describes the relationship between σ and density well (Figure 21), σ increases as density increases. Deschamps et al also showed a similar correlation (with a correlation coefficient of 0.93), although the densification in that study was via hydrostatic pressure or mechanical densification by indentation.

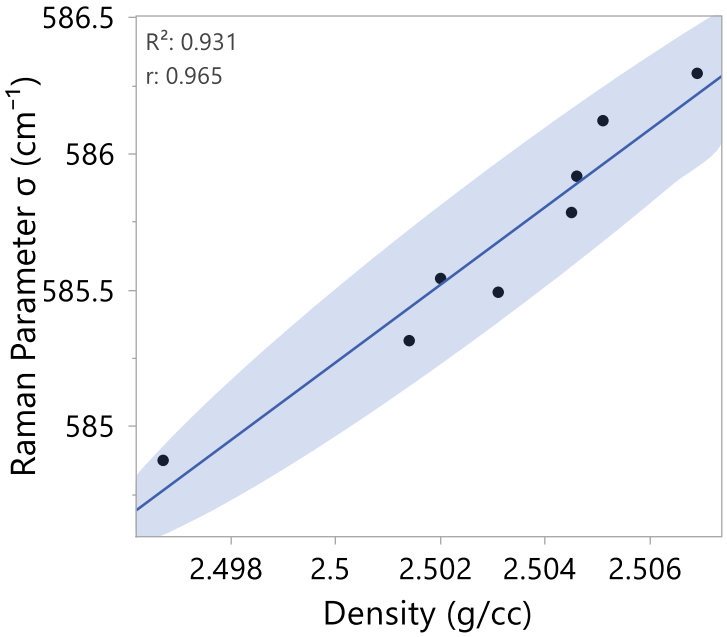

Figure 21: Raman parameter σ vs density. Straight blue line is a linear least-squares fit to the data. Shaded area represents the 95% bivariate normal density ellipse indicating very good correlation between the parameters (0.965).

The high frequency region of the Raman spectra in Fig. 18 also display subtle but systematic changes with annealing time. The baseline subtracted and normalized spectra in this frequency region can be seen in the Figure 22A, with a closer view shown in Figure 22B. This region contains the bands at 952 and 1096 cm^{-1}, which are attributed to the Si-O stretching vibration modes of the Q^2 and Q^3 spees, respectively. The normalized intensity of the 952 cm^{-1} peak decreased with annealing time as shown in Figure 22C.

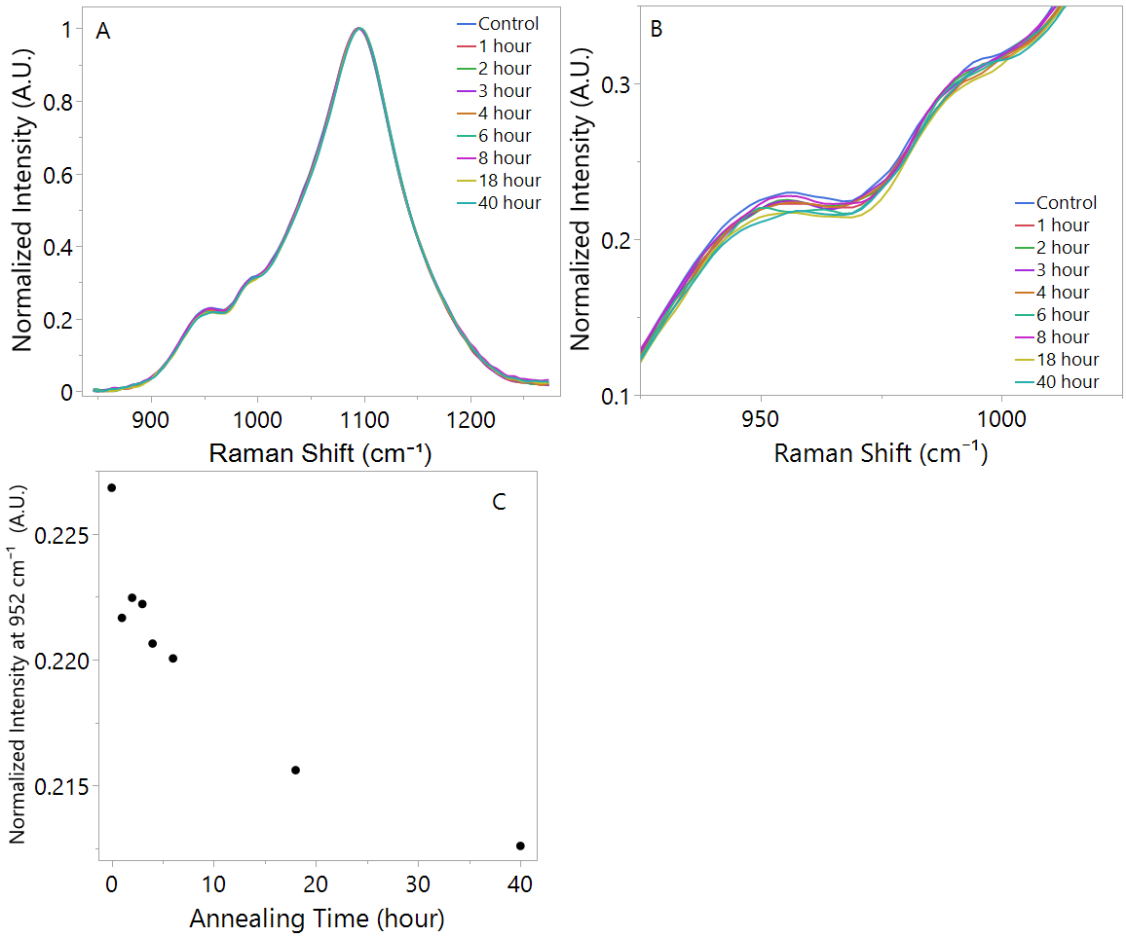

Figure 22: (A) 850cm^{-1} to 1250cm^{-1} frequency region of Raman spectra after normalization and baseline subtraction, shown for all samples. (B) Magnified view of (A) in the region around 950 cm^{-1}. (C) Intensity at 950 cm^{-1} vs annealing time, showing a monotonic decrease in intensity with increased annealing time.

These high-frequency envelopes in Fig. 22A are simulated using five Gaussian bands centered at 952 cm^{-1}, 990 cm^{-1}, 1021 cm^{-1}, 1096 cm^{-1} and 1181 cm^{-1}. An example of such a simulation is shown in Fig. 23. The change in the fractional areas of these peaks with annealing time are shown in Figures 24A-D. Since both 1021 cm^{-1} and 1180 cm^{-1} bands may be attributed to Q^4 species, the variation in the sum of the relative fractions of these two peaks with the annealing time is shown in Figure 24D. It is clear from Fig. 24 that the fractional area of the weakest band at 990 cm^{-1} and the strongest band at 1096 cm^{-1} increase and that of the other bands at 952 cm^{-1}, 1021 cm^{-1}, and 1181 cm^{-1} decrease with increasing annealing time.

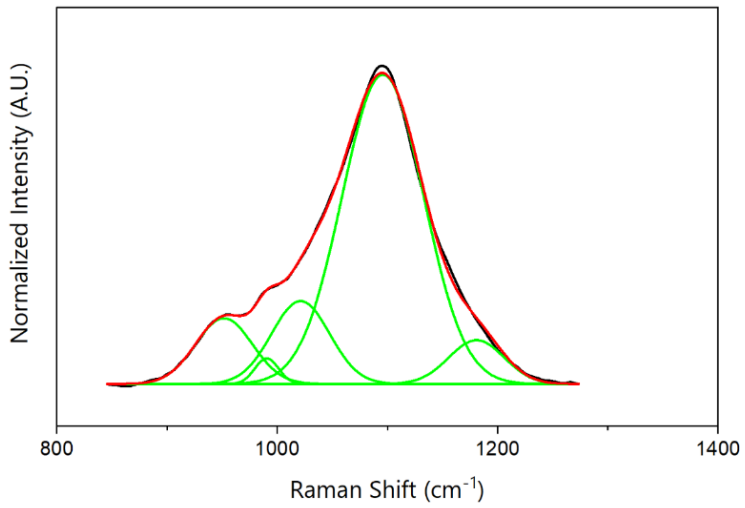

Figure 23: Example peak fitting in high frequency envelop of the Raman spectra. Five gaussian peaks fitted as described in text.

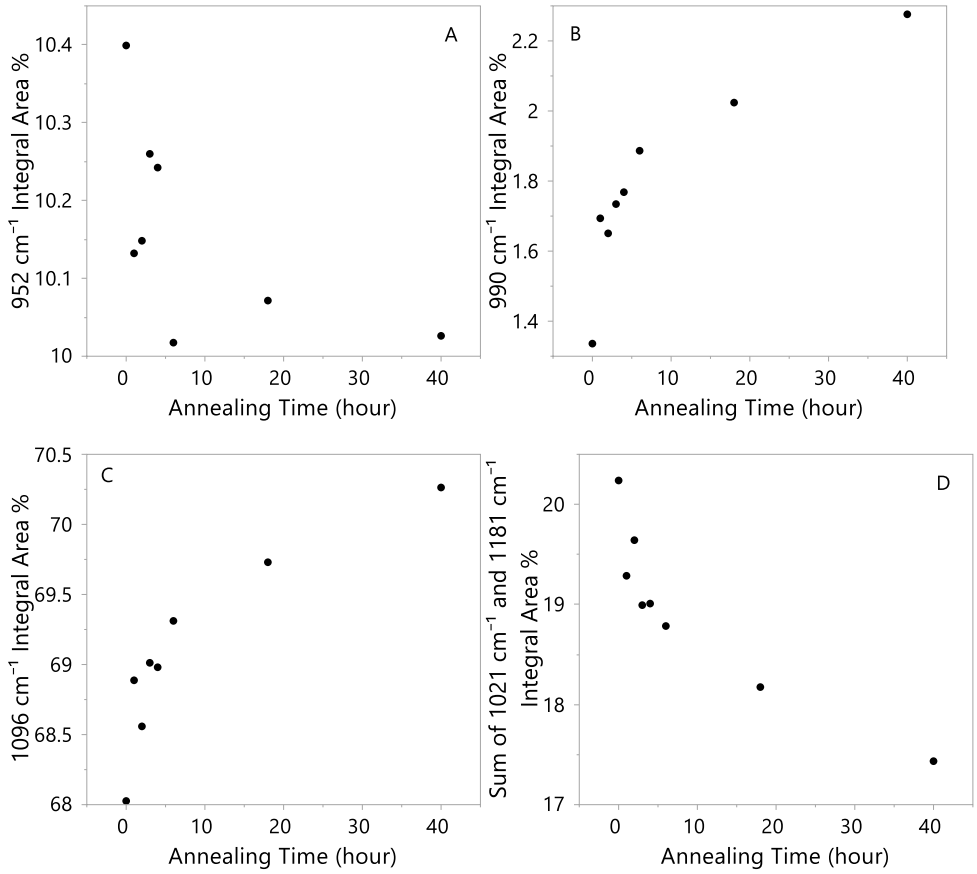

Figure 24: Annealing time dependence of fractional areas under the Raman spectral bands centered at (A) 952 cm^{-1} (B) 990 cm^{-1} (C) 1096 cm^{-1} and (D) Sum of fractional areas under 1021 cm^{-1} and 1181 cm^{-1} bands for NSG glass annealed at 500°C.

The variation of the relative fractions of various Raman bands as well as of the Raman parameter σ are compared to that of the band at 1096 cm^{-1} corresponding to the Q^3 species in Figures 25A-F. The normalized intensity of the band at 450 cm^{-1} corresponding to the Q^4 species and that of the band at 952 cm^{-1} corresponding to the Q^2 species are strongly negatively correlated with the Q^3 peak area. This result is clearly indicative of the disproportionation reaction in Equation 20.

$$2Q^3 \leftrightarrow Q^2 + Q^4 \quad \text{[Eq. 20]}$$

The negative correlation between the relative fraction of the band at 1096 cm^{-1} and the total relative fractions of the bands at 1021 and 1181 cm^{-1} points to the assignment of the latter bands to the Q^4 species. Finally, the Raman parameter σ shows a strong positive correlation with the relative fraction of the Q^3 species, which implies that as the density increases the disproportionation reaction shown in Equation 20 shifts to the left, increasing the total Q^3 species at the expense of Q^2 and Q^4 species.

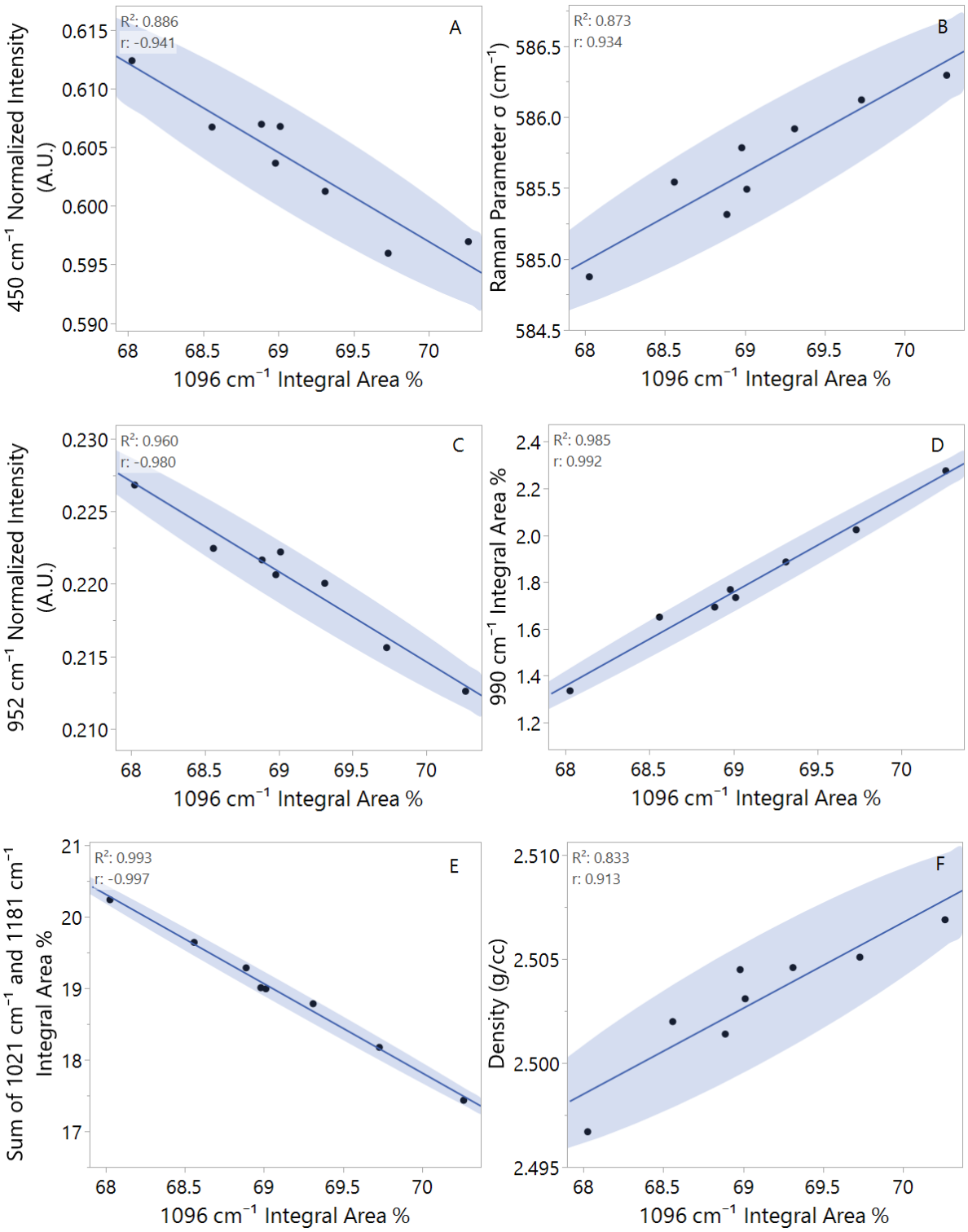

Figure 25: Correlations between various features of the measured Raman spectra and the 1096 cm^{-1} peak integral area percentage : (A) 450 cm^{-1} Normalized Intensity (B) Raman Parameter σ (C) Normalized Intensity of 952 cm^{-1} band (D) Integral area under 990 cm^{-1} band (E) Sum of areas under 1021 cm^{-1} and 1181 cm^{-1} (F) Density

When taken together, these results indicate that shear, volume (density) and structural relaxation in the highly polymerized NSG glass during annealing below Tg (i.e. aging) are strongly coupled to one another. The density increases with increasing annealing time as the glass is equilibrating to a lower fictive temperature. This density change is directly related to the Q-species disproportionation, which also drives the shear relaxation and viscous flow via Q-species exchange. This scenario is completely consistent with the results of previous high-temperature Raman and NMR spectroscopic studies of structural relaxation in supercooled modified silicate liquids above Tg [14, 39].

However, in spite of the observed correlation between the indicators of the shear, volume and structural relaxation processes, the relaxation functions for the volume and structural relaxation processes appear to differ in significant ways. This point is demonstrated in Fig. 26 where a stretched exponential relaxation function was fitted to the trends of evolution of density, and fractional areas under the Q^3 band at 1096 cm^{-1} and the Q^4 bands at 1021 cm^{-1} and 1181 cm^{-1}. The corresponding fit parameters are listed in Table 3. While the average relaxation time in all cases is ~ 300 h, the stretching exponent for the volume relaxation (~0.28) is significantly smaller than that for the structural relaxation (~0.42). The origin of this discrepancy remains unclear at this point and further studies are warranted to establish its validity over a wider temperature range.

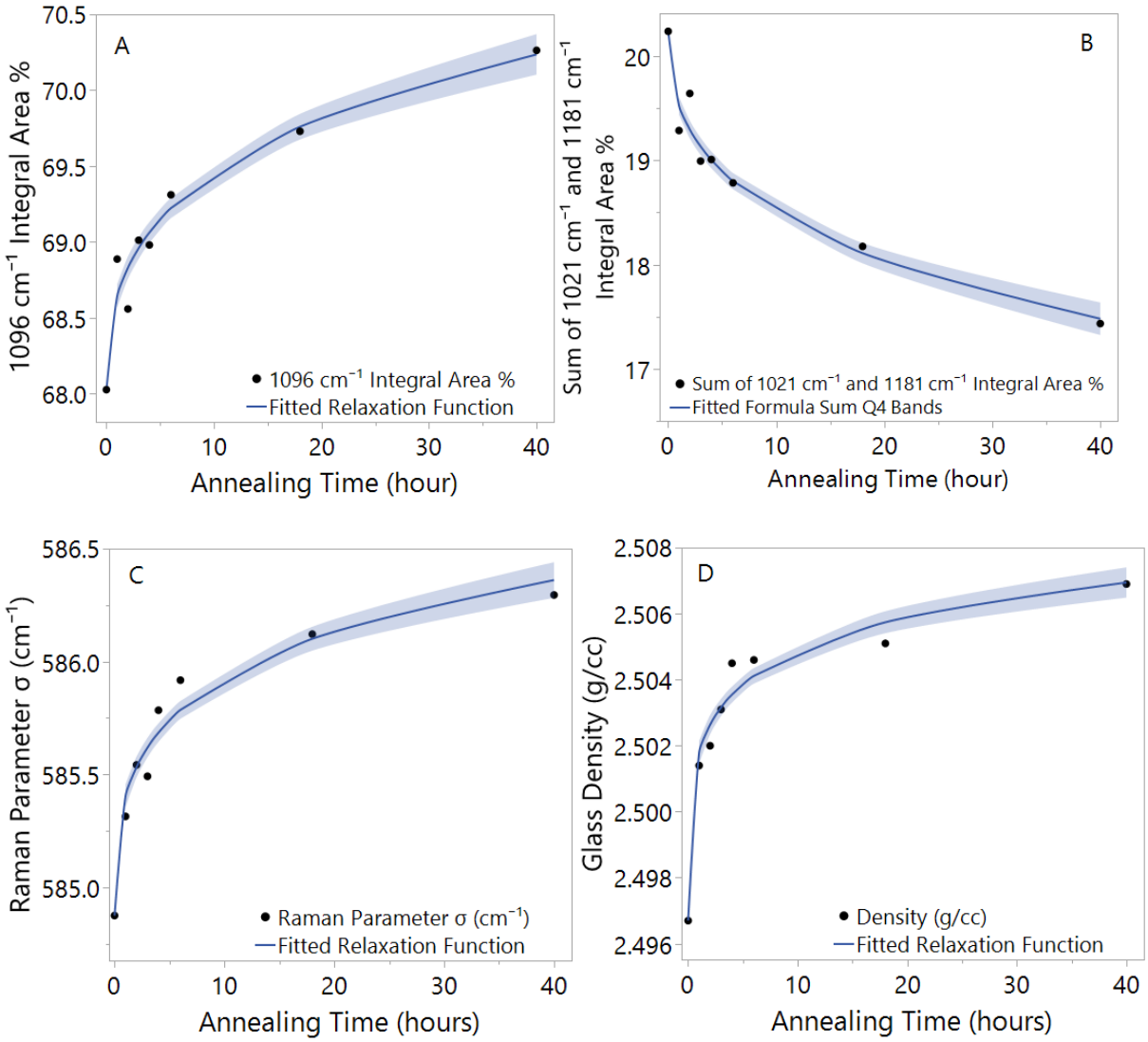

Figure 26: Non-linear fits of relaxation function for (A) Integral area % of the peak at 1096 cm^{-1} (Q^3 species) (B) Integral area % of the sum of 1021 cm^{-1} and 1181 cm^{-1} peaks (Q^4 species). (C) Raman parameter σ (cm^{-1}) (D) Density (g/cc). The shaded areas represent the standard errors of the fits.

Table 3: KWW fit parameters for fits in Fig. 26.

	β	τ	<τ> (hours)
1096 cm^{-1} Integral Area %	0.41	101	310
Sum 1021 cm^{-1} and 1181 cm^{-1} Integral Area %	0.43	110	300
Density (g/cc)	0.28	22.1	294
Raman Parameter σ (cm^{-1})	0.36	63.0	298

5. Summary

The shear, volume and structural relaxation are studied in a Na-Ca silicate glass at temperatures below the calorimetric glass transition. The results indicate strong mechanistic coupling between all three relaxation processes. Raman spectroscopic analysis demonstrates that the Q-species disproportionation reaction $2Q^3 \leftrightarrow Q^2 + Q^4$ shifts to the left upon annealing and concomitant decrease in the fictive temperature. This disproportionation reaction is responsible for the observed density relaxation as well as viscous flow in this glass. Additionally, the Raman Parameter σ that characterizes the shift in the bands at 560 cm^{-1} and 600 cm^{-1} displays a strong correlation with density, which indicates a close connection of this parameter with the Q-speciation in this glass. Finally, in spite of the temporal coupling between these three relaxation processes, the corresponding stretching exponents for the kinetics are found to be significantly different. The physical meaning of this difference remains unclear at this point, although it may be noted that previous studies have reported such differences between stress and structural relaxation and ascribed it to the different length scales and dimensionalities of the configuration landscape associated with the different relaxation processes [40].

References:

[1] Mysen B , Richet P. Silicate Glasses and Melts. 2nd ed. Amsterdam: Elsevier; 2019
[2] Varshneya AK, Mauro JC. Fundamentals of Inorganic Glasses. 3rd ed. Sheffield: Elsevier; 2019
[3] M. Anma, J. Soc. Inf. Display **9**, 95 (2001).
[4] E.D. Zanotto, J.C. Mauro, J. Non-Cryst. Solids **471** 490 (2017).
[5] W.H. Zachariasen, J. Am. Chem. Soc. **54** 3841 (1932).
[6] A.C. Wright, R.A. Hulme, D. Grimley, R.N. Sinclair, S.W. Martin, D.L. Price, F.L. Galeener, J. Non-Cryst. Solids **129** 213 (1991).
[7] F. Barmes, L. Soulard, M. Mareschal Phys. Rev. B **73** 224108 (2006).
[8] F. Galeener, J. Non-Cryst. Solids **71** 373 (1985).
[9] T. Uchino, Y. Tokuda, T. Yoko, Phys. Rev. B **58** 5322 (1998).
[10] G.N. Greaves, K.L. Ngai, Phys. Rev. B **52** 6358 (1995).
[11] H. Maekawa, T. Maekawa, K. Kawamura, T. Yokokawa, J. Non-Cryst. Solids **127** 53 (1991).
[12] V.B. Polyakov, A.A. Ariskin, A.V. Shil'dt, Glass Phys. Chem. **36** 579 (2010).
[13] M.E. Brandriss, J.F. Stebbins, Geochimica et Cosmochimica **52** 2659 (1988).
[14] B.O. Mysen, J.D. Frantz, Contrib. Mineral. Petrol. **117** 1 (1994).
[15] J. E. Dickinson, C.M. Scarfe, P. McMillan, J Geophys. Res. **95** 15675 (1990).
[16] X.Y. Xue, J.F. Stebbins, M. Kanzaki, P.F. McMillan, B. Poe, Am Miner. **79** 8 (1991).
[18] P.F. McMillan and G.H. Wolf in *Structure, Dynamics and Properties of Silicate Melts, Reviews in Mineralogy*, Vol. 32, edited by J.F. Stebbins, P.F. McMillan and D.B. Dingwell (Mineralogical Society of America, Washington DC, 1995), pp 247-315.
[19] P.F. McMillan, Ann. Rev. Earth Planet. Sci. **17** 255 (1989).
[20] S.A. Brawer, W.B. White, J. Chem. Phys. **63** 2421 (1975)
[21] B. Mysen, D. Virgo, C.M. Scarfe, Am. Miner. **65** 690 (1980)
[22] D.W. Matson, S.K. Sharma, J.A. Potts, J. Non-Cryst. Solids **58** 323 (1983) [19] Achintha M in Sustainability of Construction Materials, edited by J. Khatib Netherlands: Elsevier Science; 2016
[23] P.F. McMillan, B.T. Poe, Ph. Gillet, B. Reynard, Geochimica et Cosmochimica **58** 3653 (1994).
[24] K. Fukumi, J. Hayakawa, T. Komiyama, J. Non-Cryst. Solids **119** 297 (1990).
[25] T. Furukawa, K. Fox, W.B. White, J. Chem. Phys. **75** 3226 (1981).
[26] P.F. McMillan, Am. Miner. **69** 622 (1984)
[27] D.R. Neuville, Chem. Geo. **229** 28 (2006)
[28] C.T. Moynihan, in *Structure, Dynamics and Properties of Silicate Melts, Reviews in Mineralogy*, Vol. 32, edited by J.F. Stebbins, P.F. McMillan and D.B. Dingwell (Mineralogical Society of America, Washington DC, 1995), pp 1-19.
[29] G.W. Scherer, J Non-Cryst Solids **123** 75 (1990)
[30] G.N. Greaves and S. Sen, Adv. Phys. **56** 1 (2007).
[31] D.B. Dingwell, in *Structure, Dynamics and Properties of Silicate Melts, Reviews in Mineralogy*, Vol. 32, edited by J.F. Stebbins, P.F. McMillan and D.B. Dingwell (Mineralogical Society of America, Washington DC, 1995), pp 21-66.
[32] D.B. Dingwell, S.L. Webb, Phys. Chem. Minerals **16** 508 (1989).
[33] R.F. Lancelotti, D.R. Cassar, M. Nalin, O. Peitl, E.D. Zanotto, J Am. Ceram. Soc **104** 2066 (2021).
[34] Achintha M in Sustainability of Construction Materials, edited by J. Khatib Netherlands: Elsevier Science; 2016

[35] Francis, L. F. Materials Processing: A Unified Approach to Processing of Metals, Ceramics and Polymers. Netherlands: Elsevier Science; 2015
[36] J.C. Mauro, Y. Yue, A.J. Ellison, P.K. Gupta, D.C. Allan, Proc Natl Acad Sci. **106** 19780 (2009).
[37] J.C. Dyre, Rev. Mod. Phys. **78** 953 (2006)
[38] T. Dechamps, C. Martinet, J.L. Bruneel, B. Champagnon, J. Phys. Condens. Matter 23 035402 (2011).
[39] S. Sen, Prog. Nucl. Magn. Reson. Spectrosc. **116** 155 (2020)
[40] M. Potuzak, R.C. Welch, J.C. Mauro, J Chem. Phys. **135** 214502 (2011)